Confined states and spin polarization on a topological insulator thin film modulated by an electric potential*

Liu Yi-Man(刘一曼), Shao Huai-Hua(邵怀华), Zhou Xiao-Ying(周小英), and Zhou Guang-Hui(周光辉)†

Department of Physics and Key Laboratory for Low-Dimensional Structures and Quantum Manipulation (Ministry of Education), Hunan Normal University, Changsha 410081, *China*

(Received 9 November 2012; revised manuscript received 17 December 2012)

We study the electronic structure and spin polarization of the surface states of a three-dimensional topological insulator thin film modulated by an electrical potential well. By routinely solving the low-energy surface Dirac equation for the system, we demonstrate that confined surface states exist, in which the electron density is almost localized inside the well and exponentially decayed outside in real space, and that their subband dispersions are quasilinear with respect to the propagating wavevector. Interestingly, the top and bottom surface confined states with the same density distribution have opposite spin polarizations due to the hybridization between the two surfaces. Along with the mathematical analysis, we provide an intuitive, topological understanding of the effect.

Keywords: topological insulator thin film, electronic structure, spin polarization, electric potential

PACS: 73.50.−h, 72.80.Vp, 73.23.−b **DOI:** 10.1088/1674-1056/22/7/077310

1. Introduction

The topological insulator, a new phase of quantum matter, exhibits many interesting properties,[1,2] such as topologically protected surface or edge states, being free of backscattering, and spin-momentum locked massless Dirac cones. From these key features, it is possible to realize a number of new spintronic[3,4] and quantum computing[5,6] applications. The two-dimensional (2D) topological insulator (TI) phase was predicted to occur in HgTe quantum wells (QWs),[7] and was soon confirmed experimentally.[8] Stimulated by the quantum spin Hall effect (QSHE) in 2D TI, three-dimensional (3D) TIs have been predicted theoretically[9] and verified experimentally[10] in Bi_2Se_3 crystal. In a 3D TI, spin-orbit coupling opens an energy gap in the bulk, and results in gapless surface states which are protected by time-reversal symmetry. These 3D TIs have robust and simple surface states consisting of a single Dirac cone at the Γ-point. Much effort has concentrated on studying the unique features of the TI surface states.[11–15] However, in reality all the transport properties of the surface states are often affected by the conducting bulk states because of the unavoidable doping that is introduced by impurities and crystal lattice defects. Growing ultrathin TI films, where the bulk conduction is reduced by enhancing the surface-to-volume ratio, is a possible way to deal with this problem.[16,17]

Many of the nontrivial physical properties of TI thin films have been proposed theoretically, such as the quantum spin Hall[18,19] and quantum anomalous Hall effects,[20] strongly increased thermoelectric performance at low temperatures,[21] and excitonic superfluidity.[22] For a 3D TI thin film, finite-size confinement will lead to the interaction between the top and bottom surfaces. The hybridization develops an energy gap in the spectrum of the surface states,[18] which can be controlled by tuning the thickness of the film.[23,24] When the thickness is within 5–10 quintuple layers (QLs), the top and bottom surfaces of the thin film typically start to hybridize.[16] Recently, the full Landau-level spectrum of a 3D TI film and Hall conductivity were calculated by Zyuzin and Burkov.[25] While a peculiar phase diagram for the quantum Hall effect without Landau levels was predicted in a 3D TI thin film with an exchange field under an applied magnetic field.[26]

In this paper, we study the electronic structure and spin polarization on a 3D TI thin film modulated by an electrical potential well, i.e., like a p–n–p junction on the film surface as shown in Fig. 1. By routinely solving the low-energy 2D Dirac equation for the system, we demonstrate that there are confined surface states, in which the electron is almost localized inside the well and the electron density exponentially decays outside in real space, and their subband energy dispersions are quasilinear with respect to the propagating wavevector. Electrons at the bottom of certain energy subbands, however, are trapped in the well since their group velocity vanishes. Further, with the appreciating height of the potential, a parabolic energy subband exists because of the interplay of the externally applied potential and the hybridization between the top and bottom surfaces. For $k_y > 0$, a large proportion of electrons occupy the top surface of the film; in contrast, for $k_y < 0$, most electrons occupy the bottom surface. Interestingly, top and bottom surface states with the same density distribution

*Project supported by the National Natural Science Foundation of China (Grant No. 11274108) and the Specialized Research Fund for the Doctoral Program of Higher Education of China (Grant No. 20114306110008).

†Corresponding author. E-mail: ghzhou@hunnu.edu.cn

© 2013 Chinese Physical Society and IOP Publishing Ltd

have opposite spin polarization. The spin-surface locking is the unique characteristic of the surface state of 3D TI. In our work, the spin-surface locking is broken due to the hybridization between the top and bottom surfaces. The physical explanations for these findings are given.

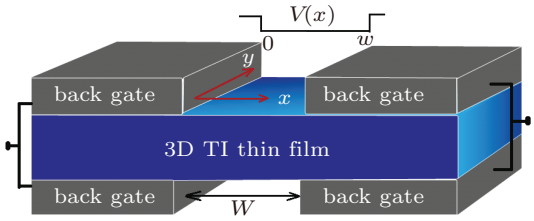


Fig. 1. (color online) Schematic illustration of the ultrathin TI film with a QW. A back gate of voltage V_0 is applied at two regions with $x<0$ and $x>W$. Electrons are confined in the QW, and the electric current flows along the y direction.

The organization of the rest of the paper is as follows: In Section 2, we present and explain the model Hamiltonian, where the bound state phase in the band spectrum is found and analyzed through directly solving the low-energy Dirac equation for the system. In Section 3, we present some numerical examples for the bound states with a discussion of the spatial-distribution of electron density and spin polarization. Finally, we summarize the results in Section 4 .

2. Model and formalism

We consider the following effective surface Hamiltonian for a 3D TI thin film in the presence of an electrostatic potential as

$$H = v_{\rm F}\boldsymbol{\tau}^z(\boldsymbol{z}\times\boldsymbol{\sigma})\cdot\boldsymbol{p}+\Delta_{\rm t}\boldsymbol{\tau}^x+V(x), \tag{1}$$

where $v_{\rm F}$ is the surface Dirac Fermi velocity, $\boldsymbol{p}=(p_x,p_y)$ is the momentum vector, $\Delta_{\rm t}$ is the hybridization matrix element (assume $\Delta_{\rm t}\geqslant 0$) which arises from the intersurface interaction between two opposing surfaces of the film and creates a gap in the energy dispersion, and $\boldsymbol{\sigma}$ and τ are Pauli matrices indicating the real spin and the surface pseudospin degrees of freedom, respectively. The potential $V(x)=V_0[\theta(-x)+\theta(x-W)]$ with height $V_0>0$ is induced by the four identical aligned back gates attached onto the top and bottom of the film, respectively, (see Fig. 1). So the top and bottom surfaces have an identical interface, where a potential well on both surfaces with width W is formed.[27] The system whose physics are described by Eq. (1) allows us to have an analytical solution for the eigenstates and sheds light on some of the general features of the problem.

Because of the momentum conservation in the y direction for the system, we look for the following general form of the corresponding complex four-component spinor wavefunction

$$\psi_\gamma(x,y)=\phi_\gamma(x){\rm e}^{{\rm i}k_y y},\ \ \gamma={\rm A,B,C,D}, \tag{2}$$

where $\psi_{\rm A}$ and $\psi_{\rm B}$ are the envelope functions for the spin-up and spin-down electrons of the top surface, respectively, while $\psi_{\rm C}$ and $\psi_{\rm D}$ are of the bottom surface. Substituting wavefunction (2) into the eigenequation corresponding to Hamiltonian (1), we obtain the coupled equations as follows:

$$-\frac{{\rm d}\phi_{\rm A}}{{\rm d}\xi}+\beta\phi_{\rm A}+\Delta\phi_{\rm D}=(\varepsilon-u)\phi_{\rm B}, \tag{3}$$

$$\frac{{\rm d}\phi_{\rm B}}{{\rm d}\xi}+\beta\phi_{\rm B}+\Delta\phi_{\rm C}=(\varepsilon-u)\phi_{\rm A}, \tag{4}$$

$$\frac{{\rm d}\phi_{\rm C}}{{\rm d}\xi}-\beta\phi_{\rm C}+\Delta\phi_{\rm B}=(\varepsilon-u)\phi_{\rm D}, \tag{5}$$

$$-\frac{{\rm d}\phi_{\rm D}}{{\rm d}\xi}-\beta\phi_{\rm D}+\Delta\phi_{\rm A}=(\varepsilon-u)\phi_{\rm C}, \tag{6}$$

where for simplicity, we have introduced the dimensionless physical quantities: $\varepsilon=EW/\hbar v_{\rm F}$ with electron energy E, $u=V(x)W/\hbar v_{\rm F}$, $\Delta=\Delta_{\rm t}W/\hbar v_{\rm F}$, $\beta=k_yW$, and $\xi=x/W$.

Decoupling Eqs. (3)–(6), one obtains

$$\frac{{\rm d}^2\phi_{\rm B}}{{\rm d}\xi^2}+\frac{u'}{\varepsilon-u}\frac{{\rm d}\phi_{\rm B}}{{\rm d}\xi}+\left[(\varepsilon-u)^2+\frac{u'\beta}{\varepsilon-u}-\beta^2-\Delta^2\right]\phi_{\rm B}+\frac{u'\Delta}{\varepsilon-u}\phi_{\rm C}=0, \tag{7}$$

$$\frac{{\rm d}^2\phi_{\rm C}}{{\rm d}\xi^2}+\frac{u'}{\varepsilon-u}\frac{{\rm d}\phi_{\rm C}}{{\rm d}\xi}+\left[(\varepsilon-u)^2-\frac{u'\beta}{\varepsilon-u}-\beta^2-\Delta^2\right]\phi_{\rm C}+\frac{u'\Delta}{\varepsilon-u}\phi_{\rm B}=0, \tag{8}$$

where u' is the derivative of the potential, namely, the Dirac δ function in our model.

The feature of the solutions for Eqs. (7) and (8) depends on u and β. Generally, the solutions are of three types:[28] (i) bound waves in the well for massless fermions arising only from the values of V_0 and k_y above the energy-dependent cutoff, and decaying exponentially outside the well; (ii) traveling waves describing free electrons and holes, as well as mixed states that occur due to the Klein tunneling of electrons to holes outside the well; and (iii) tunneling waves which are oscillatory outside the well whereas in the well they are combinations of exponentials with exponents, which correspond to holes that undergo ordinary tunneling across the potential well. However, only the type (i) solution occurs in the region of $E-k_y$ space where there are no-hole states available outside the well. This suppresses the Klein tunneling, since it depends on the electron–hole conversion at the interface. In this work, we focus on the type (i) solution, which describes electron states confined across the potential well. This type of solution describes the electron states localized inside the well and exponentially decays outside the well. The energies are in the region restricted by the curves $(E-V_0)^2<\hbar^2v_{\rm F}^2k_y^2+\Delta_t^2$ and $E^2>\hbar^2v_{\rm F}^2k_y^2+\Delta_t^2$ in E–k_y space.

For $\xi<0$, we write the solution for two components of the envelope function of Eqs. (7) and (8) as: $\phi_{\rm B}(\xi)=A_1{\rm e}^{\alpha\xi}$ and $\phi_{\rm C}(\xi)=B_1{\rm e}^{\alpha\xi}$ with arbitrary constants A_1 and B_1, where the decay constant α is given by $\alpha^2=\beta^2+\Delta^2-(\varepsilon-u_0)^2$ with $u_0=V_0W/\hbar v_{\rm F}$. Substituting these expressions for $\phi_{\rm B}$ and

ϕ_C into Eqs. (3) and (6), we obtain the other two components of the envelope function

$$\phi_A = \frac{(\alpha+\beta)A_1 + \Delta B_1}{\varepsilon - u_0} e^{\alpha\xi}$$

and

$$\phi_D = \frac{(\alpha-\beta)B_1 + \Delta A_1}{\varepsilon - u_0} e^{\alpha\xi}.$$

Meanwhile, inside the well ($0 \leqslant \xi \leqslant 1$), the solutions are of the form

$$\begin{aligned}\phi_A(\xi) &= \frac{1}{\varepsilon}\big[(D_2\kappa + \beta C_2 + \Delta G_2)\cos(\kappa\xi) \\ &\quad + (-C_2\kappa + \beta D_2 + \Delta H_2)\sin(\kappa\xi)\big], \quad (9)\\ \phi_B(\xi) &= C_2\cos(\kappa\xi) + D_2\sin(\kappa\xi), \quad (10)\\ \phi_C(\xi) &= G_2\cos(\kappa\xi) + H_2\sin(\kappa\xi), \quad (11)\\ \phi_D(\xi) &= \frac{1}{\varepsilon}\big[(H_2\kappa - \beta G_2 + \Delta C_2)\cos(\kappa\xi) \\ &\quad + (-G_2\kappa - \beta H_2 + \Delta D_2)\sin(\kappa\xi)\big], \quad (12)\end{aligned}$$

with arbitrary constants C_2, D_2, G_2, and H_2, and the parameter $\kappa^2 = \varepsilon^2 - \beta^2 - \Delta^2$. Furthermore, for $\xi > 1$, the solutions are similar to those for $\xi < 0$ but with a negative exponent: $\phi_B(\xi) = A_3 e^{-\alpha\xi}$ and $\phi_C(\xi) = B_3 e^{-\alpha\xi}$ with arbitrary constants A_3 and B_3. Consequently,

$$\phi_A(\xi) = \frac{(-\alpha+\beta)A_3 + \Delta B_3}{\varepsilon - u_0} e^{-\alpha\xi}$$

and

$$\phi_D(\xi) = \frac{(-\alpha-\beta)B_3 + \Delta A_3}{\varepsilon - u_0} e^{-\alpha\xi}.$$

The relationships among all the constants A_1, B_1, A_3, B_3, C_2, D_2, G_2, and H_2 are to be determined by the continuity conditions for the wavefunctions at the well boundaries.

By employing the continuity condition at $\xi = 0$ and $\xi = 1$, we obtain a transcendental equation for the energy spectrum of the existed bound states

$$(\kappa^2 - \varepsilon u_0)\tan\kappa = \alpha\kappa. \quad (13)$$

Replacing with the original parameters, equation (13) can be rewritten as

$$(\kappa'^2 - EV_0)\tan(W\kappa'/\hbar v_F) = \kappa'\sqrt{2EV_0 - \kappa'^2 - V_0^2}, \quad (14)$$

with $\kappa' = (E^2 - \hbar^2 v_F^2 k_y^2 - \Delta_t^2)^{1/2}$, which can be solved numerically for given parameters.

On the other hand, it is known that the spin-momentum locking for the surface of 3D TI under the modulation of potentials is different from that for a pure surface state.[29–31] Is this characteristic also kept for a 3D TI thin film surface state under an electrostatic potential? To answer this question, we rewrite the total wavefunction as

$$\psi(x,y) = \psi_1(x,y)\begin{pmatrix}1\\0\end{pmatrix} + \psi_2(x,y)\begin{pmatrix}0\\1\end{pmatrix},$$

$$\psi_i = a_i(x,y)\begin{pmatrix}1\\0\end{pmatrix} + b_i(x,y)\begin{pmatrix}0\\1\end{pmatrix},$$

with i=1, 2. Therefore, the three components of electron spin polarization can be obtained[32]

$$\begin{cases} P_x = \langle\sigma_x\rangle = 2\sum\limits_i \mathrm{Re}(a_i^* b_i) = 2\phi_A\phi_B + 2\phi_C\phi_D, \\ P_y = \langle\sigma_y\rangle = 2\sum\limits_i \mathrm{Im}(a_i^* b_i) = 0, \\ P_z = \langle\sigma_z\rangle = \sum\limits_i (|a_i|^2 - |b_i|^2) \\ \quad = |\phi_A|^2 - |\phi_B|^2 + |\phi_C|^2 - |\phi_D|^2. \end{cases} \quad (15)$$

From Eq. (15) we find that the property of spin-surface locking is broken for a 3D TI thin film due to the hybridization between the top and bottom surfaces, which is different from the approximate hard-wall boundary picture for the single surface of a 3D TI.[32,33]

3. Results and discussion

In what follows, we present some numerical examples of energy bands, envelope wavefunctions, and spatial-distributions of spin polarization for the confined states in the system with QW width $W = 200$ nm and film interface coupling strength $\Delta_t = 1$ meV[16,25] throughout the paper.

Figure 2 shows the energy E versus the wavevector k_y according to Eq. (14) for surface states confined in the QW with potential height $V_0 = 30$ meV. As seen from the (black) solid lines in the region determined by $(E - V_0)^2 < \hbar^2 v_F^2 k_y^2 + \Delta_t^2$ and $E^2 > \hbar^2 v_F^2 k_y^2 + \Delta_t^2$, we notice that there are some local energy minimums symmetrical with respect to k_y, which indicate that electrons at the bottom of the energy subband are trapped in the well since the group velocity vanishes. Electrons with $k_y = \pm 0.014$ nm^{-1} in the lower inset of Fig. 2 marked by (red) stars are trapped. Due to the existence of hybridization between two surfaces of the film, a parabolic energy subband arises in the spectrum of the bound states. We know that the hybridization develops an energy gap $\Delta E = 2\Delta_t$ at the Γ-point in the dispersion without electrical confinement.[18,23,24] Here, in the range of $V_0 - \Delta_t < E < V_0 + \Delta_t$, bound states are allowed for $k_y = 0$. This energy range produces a perfect quantized electron branch which is not intercepted by the free-particle regions. Thus, neither a free-electron nor a free-hole state can be transformed into a new bound electron state in this branch regardless of the wavevector k_y. If $V_0 < 2\Delta_t$, there is no cutoff at lower energies due to no intersection of two delimited curves. The confined states show a quasilinear versus the momentum k_y. The larger the values of k_y, the more obvious the linearity will be. This can be demonstrated by the expression of the dispersion relation. For large values of k_y, we obtained the approximate dispersion branches $E = E_n = [\hbar^2 v_F^2 (n^2\pi^2/W^2 + k_y^2) + \Delta_t^2]^{1/2}$, where n is an integer.

The upper inset of Fig. 2 shows the electron probability density $\rho = \psi^\dagger\psi$ for the confined states, with $k_y = \pm 0.02$ nm^{-1}, indicated by the (red and blue) solid circular

dots. In this figure, we see that the spatial distributions of ρ for the two confined states corresponding to the same subband but with inverse k_y completely overlap with each other, which indicates the degeneracy of the two states. The electron states are almost localized inside the well and exponentially decayed outside. The x-dependent distribution ρ is symmetric with respect to the middle of the well because ρ is an even function. Furthermore, through the analysis for more numerical examples for the system, we conclude that the probability densities with the same k_y decay faster outside the well as E decreases, while the probability densities with the same E decay slower outside the well as k_y decreases.

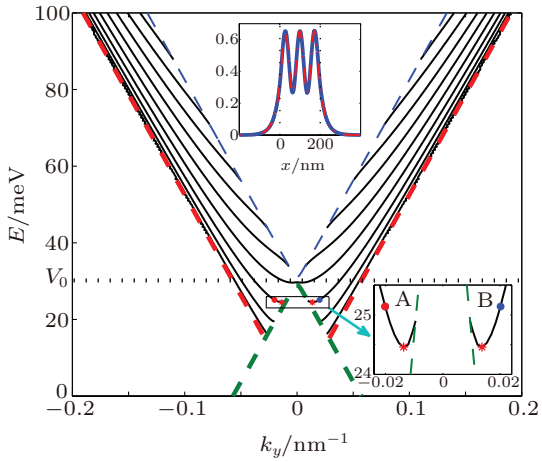


Fig. 2. (color online) The energy dispersion for the system with QW width W=200 nm, film interface coupling strength Δ_t=1 meV, and back gate potential height V_0=30 meV, where the (blue and green) dotted lines determined by $(E-V_0)^2 < \hbar^2 v_F^2 k_y^2 + \Delta_t^2$ and the (red) dotted line determined by $E^2 > \hbar^2 v_F^2 k_y^2 + \Delta_t^2$ are the regional boundary for existing bound states. The upper inset shows the spatial distribution of electron probability densities for the confined states, indicated by solid circular dots A (red) and B (blue), and the bottom inset shows a magnification of the box region in which the (red) stars indicate the local energy minimums.

Figures 3(a) and 3(b) show the x-dependent distribution of the four-component spinor wavefunctions of the bound state, indicated by the left (red) solid circular dot A and the right (blue) solid circular dot B in Fig. 2, where the (blue) solid line is for ϕ_A, (red) dashed line for ϕ_B, (green) dotted line for ϕ_C, and (black) dash-dotted line for ϕ_D. The vertical (black) dotted lines indicate the walls of the well. These two states have the same energy but inverse k_y. We can clearly see that the derivative of the four-component spinor wavefunctions is not continuous at the barrier boundaries. The distribution of a single spinor component is asymmetric because it is neither the even nor odd function of x. A large proportion of electrons with $k_y > 0$ occupy the top surface of the thin film, while for $k_y < 0$, most electrons occupy the bottom surface of the film in the QW region. The proportion of occupied electrons is just the inverse for the two states A and B. Furthermore, comparing Fig. 3(a) with Fig. 3(b), the top and bottom surface confined states with opposite spins have the same distributions of wavefunctions. For example, the spin-down wavefunction ϕ_D for $k_y = -0.02$ nm^{-1} has the same distribution as that of the spin-up wavefunction ϕ_A for $k_y = 0.02$ nm^{-1}. This characteristic is determined by the conjugated symmetry of the Hamiltonian. We rewrite the Hamiltonian as

$$H(k_x, k_y) = \begin{bmatrix} H_{11} & H_{12} \\ H_{21} & H_{22} \end{bmatrix}. \tag{15}$$

The elements of the Hamiltonian have the relation $H_{11}(k_x, k_y) = H_{22}^*(k_x, -k_y)$ in momentum space. This is the physical origin of the above feature for the four-component spinor wavefunctions. In addition, further numerical analysis of the spinor wavefunctions allow us to conclude some interesting results as follows: as E approaches V_0, the wavefunction decays faster outside the well; for $k_y > 0$, the amplitudes of the two-component spinor wavefunctions of the top surface increase and those of the bottom surface decrease, while the situation is reversed for $k_y < 0$. When $E \approx V_0$, the maxima of amplitudes is nearly equal to 1. This means that almost all electrons with $k_y > 0$ occupy the top surface, but occupy the bottom surface with $k_y < 0$.

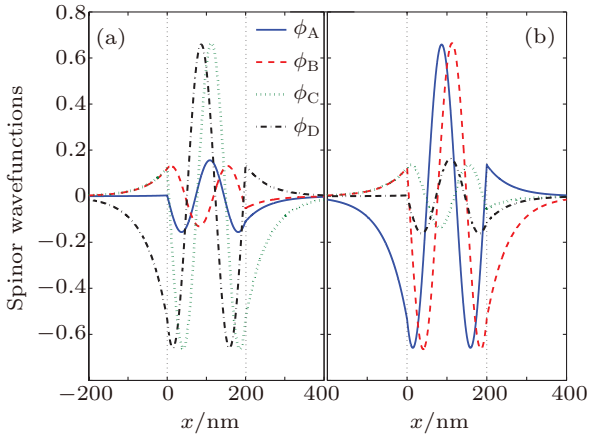


Fig. 3. (color online) The four-component spinor wavefunctions, where the (blue) solid line is for ϕ_A , the (red) dashed line ϕ_B, the (green) dotted line ϕ_C, and the (black) dash-dotted line ϕ_D of the bound state. (a) and (b) correspond to the left (red) solid circular dot A and the right (blue) solid circular dot B in Fig. 2.

Next, a numerical example for the spatial distribution of spin polarization according to Eq. (15) for $V_0 = 30$ meV is shown in Fig. 4. Figures 4(a) and 4(b) correspond to state A and B shown by the (red and blue) solid circular dots in Fig. 2, respectively. One can see that the electron spin is always polarized in the x–z plane, which is perpendicular to the surface plane of the film. The x component spin polarization P_x changes suddenly at $x = 0$ and $x = W$ because of the step electrostatic potential at the two boundaries along the x direction, and its spatial distribution is always symmetrical due to the symmetry of the system itself. The Hamiltonian in the momentum space has the inversion symmetry $H(-k_x, k_y) = H^*(k_x, k_y)$, which is reflected in P_x. However, the z-component spin polarization P_z, which is caused by the hybridization between the top and bottom surfaces, is asymmetrically distributed. On the other hand, comparing Fig. 4(a)

with Fig. 4(b), the x-component spin polarization has the same x-dependent distribution for the two states, while the z component is inverse. That is to say, if we write the spin polarization as $P_z^{\rm A}$ for state A and $P_z^{\rm B}$ for state B, respectively, we have $P_z^{\rm A} = -P_z^{\rm B}$. This result agrees with the above discussion for the spinor wavefunctions in Fig. 3. Here, $P_z^{\rm A} = -P_z^{\rm B}$ indicates that the electron states on the surface of the 3D TI thin film are of certain chirality due to time reversal symmetry. Meanwhile, the spatial distribution of spin polarization oscillates periodically. The periodicity is related to the energy subband. There are n maximum values for both P_x and P_z if the bound state is in the n-th subband. Through further numerical examples, we note that the amplitudes of P_x and P_z increase remarkably as E tends to V_0 with the same k_y, while they will decrease as k_y decrease with the same E. Hence, we may output spin-polarized electrons by using a 3D TI thin film with back gates.

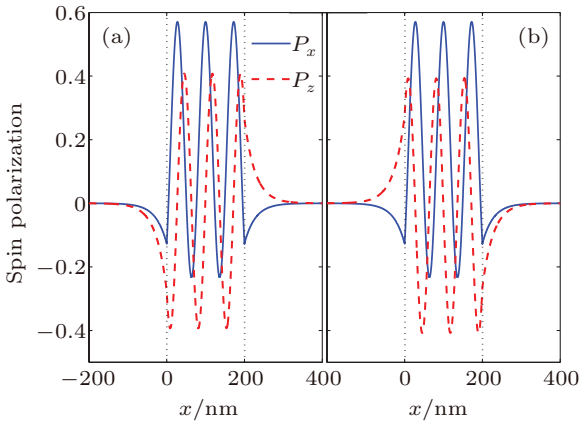


Fig. 4. (color online) The spatial distribution of spin polarization for the bound state. (a) and (b) correspond to the left (red) solid circular dot A and the right (blue) solid circular dot B in Fig. 2.

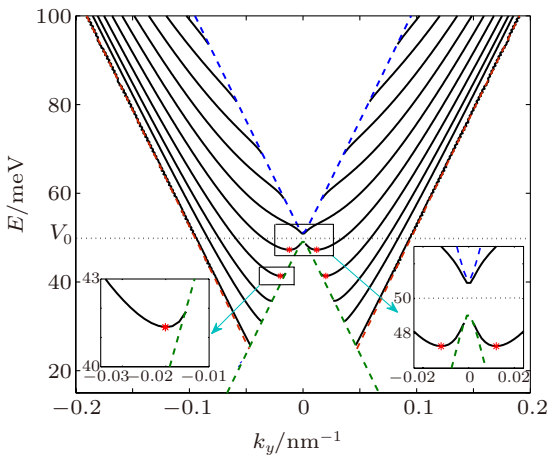


Fig. 5. (color online) The energy dispersion for the system with QW width $W = 200$ nm, film interface coupling strength $\Delta_{\rm t} = 1$ meV, and back gate potential height $V_0 = 50$ meV, where the (blue and green) dotted lines determined by $(E - V_0)^2 < \hbar^2 v_{\rm F}^2 k_y^2 + \Delta_{\rm t}^2$ and the (red) dotted line determined by $E^2 > \hbar^2 v_{\rm F}^2 k_y^2 + \Delta_{\rm t}^2$ are the regional boundaries for the existing bound states.

Moreover, we tune the back gate voltage to enhance the barrier potential $V_0 = 50$ meV. The energy spectrum is shown in Fig. 5. Comparing with Fig. 2, we can see that the region of the bound state phase can be changed by adjusting the gate voltage. However, the gate potential does not influence the time-reversal symmetry of the system; the spectrum is always symmetric with respect to wavevector k_y. The electrons with $k_y = \pm 0.012$ nm^{-1} and $k_y = \pm 0.02$ nm^{-1} in Fig. 5, marked by (red) stars, are trapped. One can also see that there are more local minimums in the dispersion relation as V_0 increases. This indicates that more electron states are trapped in the QW. However, the number of local minimums does not increase and the energy dispersion is no longer quasilinear when V_0 is hundreds of milli electron volts. Furthermore, if V_0 trends to infinity, then the energy region $V_0 - (\hbar^2 v_{\rm F}^2 + \Delta_{\rm t}^2)^{1/2} < E < V_0 + (\hbar^2 v_{\rm F}^2 + \Delta_{\rm t}^2)^{1/2}$ for confined states exists impossibly. Only region $E < V_0 - (\hbar^2 v_{\rm F}^2 + \Delta_{\rm t}^2)^{1/2}$ corresponds to free holes in the system due to Klein tunneling. The tunneling effect depends on the electron–hole conversion at the junction lines $x = 0$ and $x = W$.

4. Summary

In summary, we have demonstrated that it is possible to confine Dirac fermions on the surface of a 3D TI thin film by means of applying back gates to induce the electrostatic potentials on the film. By routinely solving the low-energy 2D Dirac equation for the system, we obtained the subband spectrum of confined surface states, in which the electron density distribution can be changed by tuning the gate voltage and the thickness of the film. We may output spin-polarized electrons by using a 3D TI thin film with back gates. These interesting findings for electrically controlled nanostructures based on a 3D TI surface can be testable in the present experimental technique, and may provide a further understanding of 3D TI surface states.

References

[1] Hasan M Z and Kane C L 2010 *Rev. Mod. Phys.* **82** 3045
[2] Qi X L and Zhang S C 2010 *Phys. Today* **63** 33
[3] Burkov A A and Hawthorn D G 2010 *Phys. Rev. Lett.* **105** 066802
[4] Culcer D, Hwang E H, Stanescu T D and Das Sarma S 2010 *Phys. Rev. B* **82** 155457
[5] Fu L and Kane C L 2008 *Phys. Rev. Lett.* **100** 096407
[6] Moore J 2009 *Nat. Phys.* **5** 378
[7] Andrei Bemeving B, Hughes T L and Zhang S C 2006 *Science* **314** 1757
[8] König M, Wiedmann S, Brüne C, Roth A, Buhmann H, Molenkamp L W, Qi X L and Zhang S C 2007 *Science* **318** 766
[9] Zhang H, Liu C X, Qi X L, Dai X, Fang Z and Zhang S C 2009 *Nat. Phys.* **5** 438
[10] Xia Y, Qian D, Hsieh D, Wray L, Pal A, Lin H, Bansil A, Grauer D, Hor Y S, Cava R J and Hasan M Z 2009 *Nat. Phys.* **5** 398
[11] Chen Y L, Analytis J G, Chu J H, Liu Z K, Mo S K, Qi X L, Zhang H J, Lu D H, Dai X, Fang Z, Zhang S C, Fisher I R, Hussain Z and Shen Z X 2009 *Science* **325** 178
[12] Hsieh D, Xia Y, Wray L, Qian D, PAl A, Dil J H, Osterwalder J, Meier F, Bihlmayer G, Kane C L, Hor Y S, Cava R J and Hasan M Z 2009 *Science* **323** 919
[13] Alpichshev Z, Analytis J G, Chu J H, Fisher I R, Chen Y L, Shen Z X, Fang A and Kapitulnik A 2010 *Phys. Rev. Lett.* **104** 016401

[14] Cheng P, Song C, Zhang T, Zhang Y, Wang Y, Jia J F, Wang J, Y. Wang Y, Zhu B F, Chen X, Ma X C, He K, Wang L L, Dai X, Fang Z, Xie X, Qi X L, Liu C X, Zhang S C and Xue Q K 2010 *Phys. Rev. Lett.* **105** 076801
[15] Yuan J H, Cheng Z, Zhang J J, Zeng Q J and Zhang J P 2012 *Chin. Phys. B* **21** 047203
[16] Zhang Y, He K, Chang C Z, Song C L, Wang L, Chen X, Jia J, Fang Z, Dai X, Shan W Y, Shen S Q, Niu Q, Qi X, Zhang S C, Ma X, and Xue Q K 2010 *Nat. Phys.* **6** 584
[17] Jin H, Song J H and Freeman A J 2011 *Phys. Rev. B* **83** 125319
[18] Liu H Z, Shan W Y, Yao W, Niu Q and Shen S Q 2010 *Phy. Rev. B* **81** 115407
[19] Liu C X, Zhang H J, Yan B, Qi X L, Frauenheim T, Dai X, fang Z and Zhang S C 2010 *Phys. Rev. B* **81** 041307(R)
[20] Yu R, Zhang W, Zhang H J, Zhang S C, Dai X and Fang Z 2010 *Science* **329** 61
[21] Ghaemi P, Mong R S K and Moore J E 2010 *Phys. Rev. Lett.* **105** 166603
[22] Seradjeh B, Moore J E and Franz M 2009 *Phys. Rev. Lett.* **103** 066402
[23] Li H, Sheng L, Sheng D N and Xing D Y 2010 *Phys. Rev. B* **82** 165104
[24] Shan W Y, Lu H Z and Shen S Q 2010 *New J. Phys.* **12** 043048
[25] Zyuzin A A and Burkov A A 2011 *Phys. Rev. B* **83** 195413
[26] Li H, Sheng L and Xing D Y 2011 *Phys. Rev. B* **84** 035310
[27] Chen J, Qin H J, Yang F, Liu J, Guan T, Qu F M, Zhang G H, Shi J R, Xie X C, Yang C L, Wu K H, Li Y Q and Lu L 2010 *Phys. Rev. Lett.* **105** 176602
[28] Milton Pereira J, Jr, Mlinar V and Peeters F M 2006 *Phys. Rev. B* **74** 045424
[29] Wu Z H, Peeters F M and Chang K 2011 *Appl. Phys. Lett.* **98** 162101
[30] Zhai F and Mu P 2011 *Appl. Phys. Lett.* **98** 022107
[31] Kong B D, Semenov Y G, Krowne C M and Kim K W 2011 *Appl. Phys. Lett.* **98** 243112
[32] Zhou X Y, Shao H H, Liu Y M, Tang D S and Zhou G H 2012 *J. Phys.: Condens. Matter* **24** 185301
[33] Shao H H, Zhou X Y, Li Y, Liu G H and Zhou G H 2011 *Appl. Phys. Lett.* **99** 153104